

A Multiple Ejecta-Circumstellar Medium Interaction Model and Its Implications for Superluminous Supernovae iPTF15esb and iPTF13dcc

Liang-Duan Liu^{1,2,3}, Ling-Jun Wang⁴, Shan-Qin Wang^{1,2,5}, and Zi-Gao Dai^{1,2}

¹*School of Astronomy and Space Science, Nanjing University, Nanjing 210093, China; dzg@nju.edu.cn*

²*Key Laboratory of Modern Astronomy and Astrophysics (Nanjing University), Ministry of Education, China*

³*Department of Physics and Astronomy, University of Nevada, Las Vegas, NV 89154, USA*

⁴*Astroparticle Physics, Institute of High Energy Physics, Chinese Academy of Sciences, Beijing 100049, China*

⁵*Department of Astronomy, University of California, Berkeley, CA 94720-3411, USA*

ABSTRACT

In this paper, we investigate two hydrogen-poor superluminous supernovae (SLSNe) iPTF15esb and iPTF13dcc whose light curves (LCs) show significant deviation from the smooth rise and fall. The LC of iPTF15esb exhibits two peaks and a post-peak plateau, and furthermore the late-time spectrum of iPTF15esb shows a strong, broad H α emission line. The early-time LC of iPTF13dcc shows a long duration bump followed by the second peak. Here we propose an ejecta-circumstellar medium (CSM) interaction model involving multiple shells/winds and use it to explain the LCs of iPTF15esb and iPTF13dcc. We find that the theoretical LCs reproduced by this model can well match the observations of iPTF15esb and iPTF13dcc. Based on our results, we infer that the progenitors have undergone multiple violent mass-loss processes before the SN explosion. In addition, we find that the variation trend of our inferred densities of the shells is consistent with that predicted by the stellar mass-loss history before an SN explosion. Further investigations for other bumpy SLSNe/SNe would shed light on their nature and provide a probe for the mass-loss history of their progenitors.

Subject headings: circumstellar matter – supernovae: general – supernovae: individual (iPTF15esb, iPTF13dcc)

1. Introduction

In the past decade, fast-developing non-targeted supernova (SN) survey programs have discovered a new class of unusual SNe whose peak absolute magnitudes M_{peak} are brighter than -21 mag. These very luminous SNe are called “superluminous supernovae (SLSNe)” (Quimby et al. 2011; Gal-Yam 2012).

It appears that SLSNe can be simply divided into two subclasses, types I and II. SLSNe I have spectra around the peaks that are lack of hydrogen absorption lines and their light curves (LCs) might be explained by the pair instability SNe (PISNe; Rakavy & Shaviv 1967; Heger & Woosley 2002; Heger et al. 2003), the ^{56}Ni -powered model, the magnetar-powered model (Kasen & Bildsten 2010; Woosley 2010; Inserra et al. 2013; Wang et al. 2015a,b; Dai et al. 2016; Wang et al. 2016a; Liu et al. 2017; Yu et al. 2017), or the ejecta-circumstellar medium (CSM) interaction model (Chevalier & Irwin 2011; Chatzopoulos et al. 2012, 2013; Ginzburg & Balberg 2012; Nicholl et al. 2014; Chen et al. 2015).

On the other hand, the spectra around the peaks of SLSNe II show strong hydrogen emission features and almost all of them show narrow and intermediate width Balmer emission lines, similar to normal SNe IIn. Previous studies (Smith & McCray 2007; Moriya et al. 2011; Chatzopoulos et al. 2012, 2013; Moriya et al. 2013) suggested that the LCs of SLSNe IIn might be powered by the interactions between the SN ejecta and the dense, hydrogen-rich, and optically thick CSM.

However, some SLSNe I (e.g., iPTF13ehe, iPTF15esb and iPTF16bad) whose late-time spectra exhibit $\text{H}\alpha$ emission lines (Yan et al. 2015, 2017) complicated the classification scheme. Yan et al. (2015) estimated that 15% of SLSNe I might have these spectral features. Among these SLSNe I that have late-time $\text{H}\alpha$ emission lines, iPTF15esb, exploded at a redshift z of 0.224, is the most striking one. Its late-time spectra show strong, broad $\text{H}\alpha$ emission lines, indicating the interaction between the SN ejecta and the hydrogen-rich CSM shell surrounding the SN progenitor. Moreover, its LC has two peaks whose luminosities are approximately equal to each other ($L_{\text{peaks}} \approx 4 \times 10^{43} \text{ erg s}^{-1}$) and a plateau lasting about 40 days. Its late-time LC decays as $L_{\text{bol}} \propto t^{-2.5}$. Another interesting case is iPTF13dcc (Vreeswijk et al. 2017) whose LC shows an initial slow decline with a duration being ~ 30 days, and then rebrightens and reaches its second peak.

Both the LCs of iPTF15esb and iPTF13dcc challenge all the models mentioned above. The decline rate of the late-time LCs powered by ^{56}Ni cascade decay with full trapping of γ rays is 0.0098 mag per day and the late-time LCs powered by a magnetar (with full trapping of γ -rays) can be described by $L_{\text{inp,mag}} \propto t^{-2}$. The magnetar model together with ^{56}Ni cascade decay with leakage of γ rays (Clocchiatti & Wheeler 1997; Wang et al. 2015a; Chen

et al. 2015) is able to explain the late-time LC of iPTF15esb, but this model cannot yield the LC showing two bright peaks and a plateau. It seems that an energy-source model involving multiple energy injections is needed to account for the exotic LCs of iPTF15esb. Wang et al. (2016b) proposed a triple-energy-source model (^{56}Ni plus magnetar plus interaction) and used it to explain the LC of iPTF13ehe. However, this model involves only one collision between the ejecta and the CSM shell and cannot produce the undulatory LCs. The model containing cooling emission and magnetar spinning-down or the ejecta-CSM interaction that has been adopted by Vreeswijk et al. (2017) to fit the double-peaked LC of iPTF13dcc cannot yet reproduce such undulations seen in the LC of iPTF15esb.

As pointed out by Yan et al. (2017), however, the spectrum and the LC seem to favor the interactions between the SN ejecta and multiple CSM shells or CSM clumps at different radii. Here we propose an ejecta-CSM interaction model involving interactions between the SN ejecta and multiple shells and stellar winds and use this model to fit the LC of iPTF15esb. The double interaction model is also promising to account for the LC of iPTF13dcc.

This paper is structured as follows. In Section 2, we give a detailed description of the model, and apply it to fit the LCs of iPTF15esb and iPTF13dcc in Section 3. Finally, we discuss our results and present our conclusions in Section 4.

2. Multiple Ejecta-CSM Interaction Model

In this section, we generalize the normal ejecta-CSM interaction model to more complicated model that involves multiple CSM shells and winds. The basic physical picture of this model is described below. The interaction of the ejecta with the pre-existing CSM results in the formation of two shock waves: a forward shock (FS) propagating through the CSM and a reverse shock (RS) sweeping up the SN ejecta (Chevalier 1982; Chevalier & Fransson 1994). The interaction provides a strong energy source by converting the kinetic energy to radiation.

Based on numerical simulations for an SN explosion, a broken power-law distribution for the density of the SN ejecta can be adopted (Matzner & McKee 1999). The density profile of the outer part ejecta is

$$\rho_{\text{NS,out}} = g_n t^{n-3} r^{-n}, \quad (1)$$

where n is the slope of the outer part ejecta, depending on the SN progenitor star, and g_n is the density profile scaling parameter, which is given by (Chevalier & Fransson 1994;

Chatzopoulos et al. 2012)

$$g_n = \frac{1}{4\pi(n-\delta)} \frac{[2(5-\delta)(n-5)E_{\text{SN}}]^{(n-3)/2}}{[(3-\delta)(n-3)M_{\text{ej}}]^{(n-5)/2}}, \quad (2)$$

where δ is the inner density profile slope. Here E_{SN} is the total SN energy, and M_{ej} is the total mass of the SN ejecta. The relation between E_{SN} and M_{ej} can be written as (Chatzopoulos et al. 2012)

$$E_{\text{SN}} = \frac{(3-\delta)(n-3)}{2(5-\delta)(n-5)} M_{\text{ej}} (x_0 v_{\text{SN}})^2, \quad (3)$$

where x_0 denotes the dimensionless radius of a break in the supernova ejecta density profile from the inner component to the outer component.

Before the SN explosion, the mass loss of a massive star could erupt several gas shells surrounding the progenitor. We assume that the density of a circumstellar shell or wind is

$$\rho_{\text{CSM},i} = q_i r^{-s_i}, \quad (4)$$

where q_i is a scaling constant, and s_i is the power-law index for CSM density profile and therefore $s_i = 2$ indicates stellar winds while $s_i = 0$ indicates uniform density shells. The subscript “i” denotes the i th collision between the ejecta and the CSM shell. For a steady wind ($s_i = 2$) with a constant pre-explosion mass loss rate \dot{M} and wind velocity v_w , we have $q = \dot{M}/(4\pi v_w)$.

The shocked CSM and shocked ejecta are separated by a contact discontinuity. The radius of the contact discontinuity R_{cd} can be described by a self-similar solution (Chevalier 1982)

$$R_{\text{cd},i} = \left(\frac{A_i g_n}{q_i} \right)^{\frac{1}{n-s_i}} t^{\frac{(n-3)}{(n-s_i)}}, \quad (5)$$

where A_i is a constant. The radii of the FS and RS are given by

$$R_{\text{FS},i}(t) = R_{\text{in},i} + \beta_{\text{FS},i} R_{\text{cd},i} \quad (6)$$

and

$$R_{\text{RS},i}(t) = R_{\text{in},i} + \beta_{\text{RS},i} R_{\text{cd},i}, \quad (7)$$

where $R_{\text{in},i}$ is the initial radius of the i th interaction (which is equal to the inner radius of the CSM density profile), β_{FS} and β_{RS} are constants representing the ratio of the shock radii to the contact-discontinuity radius R_{cd} . The values of β_{FS} and β_{RS} are determined by the values of n and s_i . They are given in Table 1 of Chevalier (1982). For $n = 7$ and $s_i = 2$, we can obtain $\beta_{\text{FS}} = 1.299$, $\beta_{\text{RS}} = 0.970$, and $A = 0.27$; for $n = 7$ and $s_i = 0$, we have $\beta_{\text{FS}} = 1.181$, $\beta_{\text{RS}} = 0.935$, and $A = 1.2$.

The interaction radii which are equal to the inner radii of the CSM density profile are given by

$$R_{\text{in},i} = R_{\text{in},i-1} + (t_{\text{tr},i} - t_{\text{tr},i-1}) \left(\frac{2(5-\delta)(n-5)E_{k,i}}{x_0^2(3-\delta)(n-3)M_{\text{ej},i}} \right)^{1/2}, \quad (8)$$

where $t_{\text{tr},i}$ is the trigger time of the i th interaction relative to time zero point. Here, we set the first interaction between ejecta and CSM as the time zero point. The kinetic energy of the i th interaction is

$$E_{k,i} = E_{k,i-1} - E_{\text{rad},i-1}, \quad (9)$$

where E_{rad} is the energy loss due to radiation. The ejecta mass of the i th interaction is

$$M_{\text{ej},i} = M_{\text{ej},i-1} + M_{\text{CSM},i-1}. \quad (10)$$

The interaction between the ejecta and the CSM would convert the kinetic energy to radiation. The luminosity input function of the forward shock is (Chatzopoulos et al. 2012)

$$L_{\text{FS},i}(t) = \frac{2\pi}{(n-s_i)^3} g_n^{\frac{5-s_i}{n-s_i}} q_i^{\frac{n-5}{n-s_i}} (n-3)^2 (n-5) \beta_{\text{FS},i}^{5-s_i} A_i^{\frac{n-5}{n-s_i}} (t+t_{\text{int},i})^{\alpha_i} \theta(t_{\text{FS,BO},i}-t), \quad (11)$$

while the reverse shock's input luminosity is (Wang et al. 2017)¹

$$L_{\text{RS},i}(t) = 2\pi \left(\frac{A_i g_n}{q_i} \right)^{\frac{5-n}{n-s_i}} \beta_{\text{RS},i}^{5-n} g_n \left(\frac{n-5}{n-3} \right) \left(\frac{3-s_i}{n-s_i} \right)^3 (t+t_{\text{int},i})^{\alpha_i} \theta(t_{\text{RS},*,i}-t), \quad (12)$$

where $\theta(t_{\text{RS},*}-t)$ and $\theta(t_{\text{FS,BO}}-t)$ represent the Heaviside step function that control the end times of FS and RS, respectively, and $t_{\text{int},i} \approx R_{\text{in},i}/v_{\text{SN},i}$ is the time when the ejecta-CSM interaction begins. The temporal index is $\alpha_i = (2n+6s_i-ns_i-15)/(n-s_i)$. Here we fix $n=7$. Consequently, we have $\alpha_i = -0.143$ for the shell ($s_i=0$), and $\alpha_i = -0.6$ for the steady wind ($s_i=2$).

The RS termination timescale $t_{\text{RS},*}$ is the time once the RS sweeps up all available ejecta (Chatzopoulos et al. 2012, 2013)

$$t_{\text{RS},*,i} = \left[\frac{v_{\text{SN},i}}{\beta_{\text{RS},i} (A_i g_n / q_i)^{\frac{1}{n-s_i}}} \left(1 - \frac{(3-n)M_{\text{ej},i}}{4\pi v_{\text{SN},i}^{3-n} g_n} \right)^{\frac{1}{3-n}} \right]^{\frac{n-s_i}{s_i-3}}. \quad (13)$$

¹For reverse shock luminosity we use the expression given by Wang et al. (2017), instead of that given by Chatzopoulos et al. (2012). See Wang et al. (2017) for more details.

Under the same assumption, the FS terminates when the optically thick part of the CSM is swept up. The termination timescale of the FS, being approximately equal to the time of FS breakout $t_{\text{FS,BO},i}$, is given by (Chatzopoulos et al. 2012, 2013)

$$t_{\text{FS,BO},i} = \left\{ \frac{(3 - s_i) g_i^{(3-n)/(n-s_i)} [A_i g_n]^{(s_i-3)/(n-s_i)}}{4\pi \beta_{\text{FS},i}^{3-s_i}} \right\}^{\frac{n-s_i}{(n-3)(3-s_i)}} M_{\text{CSM,th},i}^{\frac{n-s_i}{(n-3)(3-s_i)}}, \quad (14)$$

where $M_{\text{CSM,th},i}$ is the mass of optically thick CSM

$$M_{\text{CSM,th},i} = \int_{R_{\text{in},i}}^{R_{\text{ph},i}} 4\pi r^2 \rho_{\text{CSM},i} dr. \quad (15)$$

Here $R_{\text{ph},i}$ denotes the photospheric radius of the i th CSM shell, located at the optical depth $\tau = 2/3$ under Eddington's approximation. $R_{\text{ph},i}$ is given by

$$\tau = \int_{R_{\text{ph},i}}^{R_{\text{out},i}} \kappa_i \rho_{\text{CSM},i} dr = \frac{2}{3}, \quad (16)$$

where κ is the optical opacity of the CSM and $R_{\text{out},i}$ is the radius of the outer boundary of the CSM. $R_{\text{out},i}$ can be determined by

$$M_{\text{CSM},i} = \int_{R_{\text{in},i}}^{R_{\text{out},i}} 4\pi r^2 \rho_{\text{CSM},i} dr. \quad (17)$$

Both the FS and the RS heat the interacting material. The total luminosity input from the FS and RS can be written as

$$L_{\text{inp,CSM},i}(t) = \epsilon_i [L_{\text{FS},i}(t) + L_{\text{RS},i}(t)], \quad (18)$$

where ϵ_i is the conversion efficiency from the kinetic energy. Chatzopoulos et al. (2012) assumed that $\epsilon = 100\%$, which is unrealistic in the actual situation, especially in the $M_{\text{CSM}} \ll M_{\text{ej}}$ case. Due to the poor knowledge of the process of converting the kinetic energy to radiation, for simplicity, we set ϵ_i as a free parameter.

Because the expansion velocity of the CSM is much lower than the typical velocity of the SN ejecta, Chatzopoulos et al. (2012) assumed a fixed photosphere inside the CSM. Under this assumption, the output bolometric LC can be written as

$$L_i(t) = \frac{1}{t_{\text{diff},i}} \exp\left[-\frac{t}{t_{\text{diff},i}}\right] \int_0^t \exp\left[\frac{t'}{t_{\text{diff},i}}\right] L_{\text{inp,CSM},i}(t') dt', \quad (19)$$

where $t_{\text{diff},i}$ is the diffusion timescale in the optically thick CSM. The diffusion timescales of the i th interaction can be written as

$$t_{\text{diff},i} = \sum_{j=i}^N \frac{\kappa_j M_{\text{CSM,th},j}}{\beta c R_{\text{ph}}}. \quad (20)$$

where $\beta = 4\pi^3/9 \simeq 13.8$ is a constant (Arnett 1982), and c is the speed of light.

In this multiple interaction model, the theoretical bolometric LC of N times interactions can be described as

$$L_{\text{tot}}(t) = \sum_{i=1}^N L_i(t). \quad (21)$$

We assume that the bolometric luminosity comes from the blackbody emission from the photosphere whose radius is R_{ph} , and therefore the temperature in our model can be estimated by

$$T = \left(\frac{L_{\text{tot}}}{4\pi R_{\text{ph}}^2 \sigma_{\text{SB}}} \right)^{1/4}, \quad (22)$$

where σ_{SB} is the Stefan-Boltzmann constant. By assuming a stationary photosphere, we have $T \propto L_{\text{tot}}^{1/4}$.

3. Modeling the light curves of SLSNe with multiple peaks

In this section, we use the model described above to fit the bolometric light curves of iPTF15esb and iPTF13dcc. In order to derive the best-fitting parameters and determine the ranges of relevant parameters, we develop a Markov Chain Monte Carlo (MCMC) method that can minimize the values of χ^2 divided by the number of degree of freedom (χ^2/dof) for the multiple ejecta-CSM interaction model and employ this model to fit the LCs of iPTF15esb and iPTF13dcc.

To reduce the number of free parameters in our calculations, we fix several parameters. We adopt the power-law index of the outer density profile $n = 7$ as an approximation for Type I SNe (Chevalier 1982), and the inner density slope $\delta = 0$.

The free parameters in our model are the opacities of the CSM shells and winds κ , the mass of the SN ejecta M_{ej} , the total mass of the CSM M_{CSM} , the density of the CSM at the interaction radius $\rho_{\text{CSM,in}}$, the interaction radius (the inner radius of CSM) R_{in} , the conversion efficiency from the kinetic energy to radiation ϵ , the time of the collision between the SN ejecta and the CSM shells t_{tr} .

The opacities of the CSM shells and winds κ are related to their composition and temperatures. For hydrogen-poor matter, the dominant source of opacity is electron scattering, $\kappa = 0.06 - 0.2 \text{ cm}^2 \text{ g}^{-1}$ (see the references listed in Wang et al. 2015b). For hydrogen-rich matter, $\kappa = 0.33 \text{ cm}^2 \text{ g}^{-1}$, which is the Thomson electron scattering opacity for fully ionized material with the solar metallicity (Moriya et al. 2011; Chatzopoulos et al. 2012).

3.1. iPTF15esb

It is reasonable to assume that there are at least three collisions between the SN ejecta and the CSM shells since the LC of iPTF15esb shows two prominent peaks and a plateau. In this scenario, the interaction between the SN ejecta and the stellar wind (i.e., $s_1 = 2$) powers the first peak of the LC of iPTF15esb while the second peak and the plateau are powered by the interactions between the SN ejecta and CSM shells ($s_2 = s_3 = 0$) at different radii.

The composition of the first and second CSM shells cannot be well constrained since no hydrogen emission lines in the early-time spectra of iPTF15esb have been detected. On the other hand, the strong, broad H α emission at ~ 70 days after the first LC peak might be prompted by the interaction between the ejecta and a hydrogen-rich shell. Therefore, the values of the opacity of the first and second CSM shells κ_1 and κ_2 can be fixed to be $0.06 - 0.2 \text{ cm}^2 \text{ g}^{-1}$ or $0.33 \text{ cm}^2 \text{ g}^{-1}$, and the value of the opacity of the third CSM shell κ_3 is supposed to be $0.33 \text{ cm}^2 \text{ g}^{-1}$. By analyzing FeII 5169 Å line, Yan et al. (2017) found that the photospheric velocity around the first peak of iPTF15esb is $v_{\text{ph}} \approx 17,800 \text{ km s}^{-1}$ which can be set to be the value of the characteristic velocity v_{SN} of the SN ejecta.

The theoretical LC of iPTF15esb is shown in Figure 1. The best-fitting parameters and the corresponding confidence contour corners of iPTF15esb are shown in Table 1 and Figure 2, respectively. We find that the multiple interaction model can explain the bumpy LC of iPTF15esb well ($\chi^2/\text{dof} = 1.71$) and the parameters are reasonable. The derived physical parameters of the CSM shells and the wind are listed in Table 2. The masses of the optically thick part of the CSM shells $M_{\text{CSM,th}}$, which are close to their total mass, can be calculated. The termination timescales of the FS and the RS can also be determined. The optical depth of CSM $\tau_{\text{CSM}} > 1$, indicating that these shells are opaque.

Provided that the velocity of the shells v_{shell} is $\sim 100 \text{ km s}^{-1}$ and using $t_{\text{shell}} \approx R_{\text{in}}/v_{\text{shell}}$, we can obtain the time when the progenitor expelled the CSM shells before explosion. We infer that the progenitor of iPTF15esb has undergone at least two violent shell eruption processes at 6.69, and 16.34 years before the SN explosion, respectively, then experienced a

wind-like mass loss whose mass-loss rate (\dot{M}) is $0.19 - 1.9M_{\odot} \text{ yr}^{-1}$.²

3.2. iPTF13dcc

Vreeswijk et al. (2017) used a model combining the cooling emission from an shock-heated extended envelope (Piro 2015) and energy injection from a magnetar or an ejecta-CSM interaction to fit the LC of iPTF13dcc. While this model is plausible, we suggest that the double-collision model is also a possible model accounting for the LC of iPTF13dcc. In our scenario, the early-time bump of iPTF13dcc might be powered by the first collision between the ejecta and the CSM shell, while the second collision at larger radius powers the late-time rebrightening of iPTF13dcc.

The early bump and the late-time rebrightening of iPTF13dcc are powered by the interactions between the SN ejecta and CSM shells at different radii, in which $s_1 = s_2 = 0$ is adopted. In our fitting, we adopt the expansion velocity $v_{\text{SN}} = 10,000 \text{ km s}^{-1}$, which is the same as Vreeswijk et al. (2017). We assume the opacities of the first and second CSM shells $\kappa_1 = \kappa_2 = 0.2 \text{ cm}^2 \text{ g}^{-1}$.

The theoretical LC of iPTF13dcc is shown in Figure 3. The best-fitting parameters and the corresponding confidence contour corners of iPTF13dcc are shown in Table 1 and Figure 4, respectively. The multiple-collision model can match the unusual light curve of iPTF13dcc ($\chi^2/\text{dof} = 2.25$). The ejecta mass is $M_{\text{ej}} = 14.2M_{\odot}$, and the masses of CSM shells associated with the first and second collisions are $7.1M_{\odot}$ and $18.3M_{\odot}$, respectively. Adopting $t_{\text{shell}} \approx R_{\text{in}}/v_{\text{shell}}$ and $v_{\text{shell}} \sim 100 \text{ km s}^{-1}$, we can infer that the two shells had been expelled at 1.55 and 21.72 years before the explosion, respectively.

Due to lacking the data before the maximum brightness of the early bump of iPTF13dcc, it is difficult to determine the rise time of the first bump. Based on Table 2 and Figure 3, we find that the rise time of the early bump depends on the forward-shock termination timescale of the first interaction $t_{\text{FS,BO}} = 17.8 \text{ days}$ while the decline rate of the late-time LC is determined by the reverse shock of the second collision.

² $\dot{M} = 4\pi r^2 \rho(r) v_w$, where $\rho(r)$ is the average density at a radius r , and $v_w \approx 100 - 1,000 \text{ km s}^{-1}$ is the terminal velocity of stellar wind of a hydrogen-poor star (He star; Smith 2014).

3.3. The factors influencing the LC features

The observed properties of a core collapse SN are determined by several physical parameters, including the mass of ejecta M_{ej} , the kinetic energy of the SN ejecta E_K , the composition of the ejecta, and the structure of the envelope of the progenitor at the time of explosion. These properties result in different types of observed SNe. The LCs of some multi-peaked SNe show evidence of multiple interactions between the SN ejecta and the pre-existing CSM shells. In the interaction model, several parameters related to the CSM, e.g., the mass of CSM M_{CSM} , the density profile of the CSM, CSM composition, must be taken into account. Different parameters would lead to different observational features.

The CSM properties are directly reflected by the LC shape. As shown in Figures 1 and 3, the luminosities provided by the forward shocks are usually larger than that provided by the reverse shocks. The peak times of bumps depend on the timescales of the forward shocks $t_{\text{FS,BO}}$, while the reverse shock affects the final decline rate. Less massive CSM tends to power narrower LC and the larger CSM density results in a slower decline. The peak luminosity is sensitive to the ejecta mass M_{ej} , so the explosion of a more massive star yields a brighter peak.

4. Discussion and Conclusions

Massive stars could be unstable and experience mass losses in the form of eruptions in the final stage of their lives (see, [Smith 2014](#) and the references therein). [Ofek et al. \(2014\)](#) pointed out that more than 50% of the progenitors of type IIn SNe have experienced at least one pre-explosion eruption. In several cases, the progenitors of SNe could expel at least two shells and/or winds. Thus, it is expected that the interactions between the ejecta and multiple shells/winds would power a bumpy LCs showing two or more peaks.

In this paper, we have studied two such bumpy SNe, iPTF15esb and iPTF13dcc, which show the undulation features that clearly deviate from the smooth rising and fading. the LC of iPTF15esb has two peaks and a post-peak plateau, while the LC of iPTF13dcc shows an early-time bump and a late-time rebrightening. All the previous energy-source models cannot account for these exotic features. We suggested that the LC undulations of iPTF15esb could arise from SN ejecta interacting with multiple dense CSM shells, which may be expelled by the eruptions of the progenitors. The interaction model for the LC of iPTF15esb is also favored by the broad $\text{H}\alpha$ emission lines in the late-time spectra which might be produced by the interaction of SN ejecta with hydrogen-rich CSM shell located at a large distance from the progenitor star and was ejected by the progenitor star about 16.4 years before explosion.

To solve these problems, we generalize the “single” ejecta-CSM interaction model to the multiple interaction model involving multiple CSM shells and/or winds. By employing this new model to fit the LC of iPTF15esb, we got rather good results and found that the first peak of the LC of iPTF15esb might be powered by the interaction between the SN ejecta and stellar wind while both the second peak and the plateau might be powered by the two CSM shells at different radii. By fitting the LC, we found that the masses expelled by the progenitor of iPTF15esb are $0.49 M_{\odot}$ and $1.46 M_{\odot}$ and that the mass-loss rate (\dot{M}) of the wind is $0.19 - 1.9 M_{\odot} \text{ yr}^{-1}$, which is comparable to that of SN 1994W ($\dot{M} \sim 0.2 M_{\odot} \text{ yr}^{-1}$, Chugai et al. 2004), SN 1995G ($\dot{M} \sim 0.1 M_{\odot} \text{ yr}^{-1}$, Chugai & Danziger 2003), and iPTF13z ($\dot{M} \sim 0.1 - 2 M_{\odot} \text{ yr}^{-1}$, Nyholm et al. 2017).

Furthermore, we also fitted the double-peaked LC of iPTF13dcc using this model and got rather satisfactory results. In this fit, the LC of iPTF13dcc was powered by the interactions between the ejecta and two CSM shells whose masses are $18.3 M_{\odot}$ and $7.1 M_{\odot}$, respectively. This positive result suggests that this model is also promising to account for the LCs of several double-peak SLSNe/SNe (e.g., Nicholl et al. 2016; Roy et al. 2016; Vreeswijk et al. 2017).

It is necessary to discuss the origin of the shells expelled by the progenitors of iPTF15esb and iPTF13dcc. Several models have been proposed to explain the violent pre-supernova eruptions. Woosley et al. (2007) and Woosley (2017) suggested that a very massive progenitor may undergo several episodes of pulsational pair instabilities and eject several massive shells before the SN explosion. The second possible origin is related to the binary interaction in which model the shells ejected by the progenitor are supposed to be formed by the large mass ejections from the progenitor interacting with its companion star (Podsiadlowski et al. 1992). In these successive collisions, the masses of the CSM shells decrease from the outermost shell (the first eruption) to innermost shell (the final eruption) but their density increases (since the densities of the interior of the progenitors are larger than that of the exterior). This property is consistent with the variation trend of our inferred densities of the ejected shells and wind of the progenitors of iPTF15esb and iPTF13dcc.

The mass loss of the progenitor of an SN is an important process of stellar evolution. However, our understanding of the stellar mass loss mechanism remains incomplete. Further investigations for SLSNe/SNe like iPTF15esb and iPTF13dcc should shed light on the nature of the mass-loss history of their progenitors.

We would like to thank an anonymous referee for constructive suggestions that have allowed us to improve our manuscript significantly. We also thank Hai Yu, Weikang Zheng, Bing Zhang, Can-Min Deng, and Xue-Feng Wu for helpful discussions. This work was

supported by the National Basic Research Program (“973” Program) of China (grant no. 2014CB845800), the National Key R&D Program of China (grant no. 2017YFA0402600) and the National Natural Science Foundation of China (grant no. 11573014). L.J.W. was also supported by the National Program on Key Research and Development Project of China (grant no. 2016YFA0400801). L.D.L. and S.Q.W. are supported by China Scholarship Program to conduct research at UNLV and UCB, respectively.

REFERENCES

- Arnett, W. D. 1982, *ApJ*, 253, 785
- Chatzopoulos, E., Wheeler, J. C., & Vinko, J. 2012, *ApJ*, 746, 121
- Chatzopoulos, E., Wheeler, J. C., Vinko, J., Horvath, Z. L., & Nagy, A. 2013, *ApJ*, 773, 76
- Chen, T.-W., Smartt, S. J., Jerkstrand, A., et al. 2015, *MNRAS*, 452, 1567
- Chevalier, R. A. 1982, *ApJ*, 258, 790
- Chevalier, R. A., & Fransson, C. 1994, *ApJ*, 420, 268
- Chevalier, R. A., & Irwin, C. M. 2011, *ApJ*, 729, L6
- Chugai, N. N., & Danziger, I. J. 2003, *Astronomy Letters*, 29, 649
- Chugai, N. N., Blinnikov, S. I., Cumming, R. J., et al. 2004, *MNRAS*, 352, 1213
- Clocchiatti, A., & Wheeler, J. C. 1997, *ApJ*, 491, 375
- Dai, Z. G., Wang, S. Q., Wang, J. S., Wang, L. J., & Yu, Y. W. 2016, *ApJ*, 817, 132
- Gal-Yam, A. 2012, *Science*, 337, 927
- Ginzburg, S., & Balberg, S. 2012, *ApJ*, 757, 178
- Heger, A., Fryer, C. L., Woosley, S. E., Langer, N., & Hartmann, D. H. 2003, *ApJ*, 591, 288
- Heger, A., & Woosley, S. E. 2002, *ApJ*, 567, 532
- Insera, C., Smartt, S. J., Jerkstrand, A., et al. 2013, *ApJ*, 770, 128
- Kasen, D., & Bildsten, L. 2010, *ApJ*, 717, 245
- Liu, L.-D., Wang, S.-Q., Wang, L.-J., Dai, Z.-G., Yu, H., & Peng, Z.-K. 2017, *ApJ*, 842, 26

- Matzner, C. D., & McKee, C. F. 1999, *ApJ*, 510, 379
- Moriya, T. J., Blinnikov, S. I., Tominaga, N., et al. 2013, *MNRAS*, 428, 1020
- Moriya, T., Tominaga, N., Blinnikov, S. I., Baklanov, P. V., & Sorokina, E. I. 2011, *MNRAS*, 415, 199
- Nicholl, M., Berger, E., Smartt, S. J., et al. 2016, *ApJ*, 826, 39
- Nicholl, M., Smartt, S. J., Jerkstrand, A., et al. 2014, *MNRAS*, 444, 2096
- Nyholm, A., Sollerman, J., Taddia, F., et al. 2017, *A&A*, 605, 6
- Ofek, E. O., Sullivan, M., Shaviv, N. J., et al. 2014, *ApJ*, 789, 104
- Piro, A. L. 2015, *ApJL*, 808, L51
- Podsiadlowski, P., Joss, P. C., & Hsu, J. J. L. 1992, *ApJ*, 391, 246
- Quimby, R. M., Kulkarni, S. R., Kasliwal, M. M., et al. 2011, *Nature*, 474, 487
- Rakavy, G., & Shaviv, G. 1967, *ApJ*, 148, 803
- Roy, R., Sollerman, J., Silverman, J. M., et al. 2016, *A&A*, 596, 67
- Smith, N. 2014, *ARA&A*, 52, 487
- Smith, N., & McCray, R. 2007, *ApJL*, 671, L17
- Vreeswijk, P. M., Leloudas, G., Gal-Yam, A., et al. 2017, *ApJ*, 835, 58
- Wang, L. J., Wang, S. Q., Dai, Z. G., et al. 2016a, *ApJ*, 821, 22
- Wang, L. J., Wang, X. F., Cano, Z., et al. 2017, *arXiv:1712.07359*
- Wang, S. Q., Liu, L. D., Dai, Z. G., Wang, L. J., & Wu, X. F. 2016b, *ApJ*, 828, 87
- Wang, S. Q., Wang, L. J., Dai, Z. G., & Wu, X. F. 2015a, *ApJ*, 807, 147
- Wang, S. Q., Wang, L. J., Dai, Z. G., & Wu, X. F. 2015b, *ApJ*, 799, 107
- Woosley, S. E. 2010, *ApJL*, 719, L204
- Woosley, S. E. 2017, *ApJ*, 836, 244
- Woosley, S. E., Blinnikov, S., & Heger, A. 2007, *Nature*, 450, 390

Yan, L., Lunnan, R., Perley, D. A., et al. 2017, *ApJ*, 848, 6

Yan, L., Quimby, R., Ofek, E., et al. 2015, *ApJ*, 814, 108

Yu, Y.-W., Zhu, J.-P., Li, S.-Z., Lü, H.-J., & Zou, Y.-C. 2017, *ApJ*, 840, 12

Table 1: The fitting parameters for iPTF15esb and iPTF13dcc

i th interaction	s	κ ($\text{cm}^2 \text{g}^{-1}$)	M_{ej} (M_{\odot})	M_{CSM} (M_{\odot})	$\rho_{\text{CSM,in}}^{\text{b}}$ ($10^{-13} \text{g cm}^{-3}$)	ϵ^{c}	t_{tr} (days)	R_{in} (10^{15}cm)
iPTF15esb								
1	2	0.2	$3.92^{+0.24}_{-0.52}$	$0.49^{+0.05}_{-0.03}$	$20.1^{+1.9}_{-5.1}$	$0.42^{+0.03}_{-0.02}$	-8.5	$0.22^{+0.04}_{-0.02}$
2	0	0.2	4.41 ^a	$1.46^{+0.24}_{-0.24}$	$4.35^{+0.45}_{-0.16}$	$0.19^{+0.02}_{-0.02}$	5.2	2.11 ^d
3	0	0.33	5.87 ^a	$2.14^{+0.13}_{-0.05}$	$0.43^{+0.05}_{-0.02}$	$0.12^{+0.01}_{-0.01}$	24.2	5.15 ^d
iPTF13dcc								
1	0	0.2	$14.22^{+0.92}_{-2.51}$	$7.09^{+0.70}_{-2.20}$	$12.0^{+7.3}_{-6.2}$	$0.46^{+0.06}_{-0.07}$	-73.79	$0.1^{+0.17}_{-0.05}$
2	0	0.2	21.31 ^a	$18.25^{+3.97}_{-5.44}$	$6.4^{+5.62}_{-2.28}$	$0.11^{+0.04}_{-0.01}$	-24.69	6.85 ^d

a. $M_{\text{ej},2}$ and $M_{\text{ej},3}$ are not fitting parameters, but calculated by Equation (10).

b. $\rho_{\text{CSM,in}}$ is the density of the CSM at radius $R = R_{\text{in}}$.

c. ϵ is the conversion efficiency from the kinetic energy to radiation.

d. $R_{\text{in},2}$ and $R_{\text{in},3}$ are not fitting parameters, but calculated by Equation (8).

Table 2: The derived physical parameters

i th interaction	$M_{\text{CSM,th}}^{\text{a}}$ (M_{\odot})	$t_{\text{FS,BO}}$ (days)	$t_{\text{RS,*}}$ (days)	t_{diff} (days)	$\tau_{\text{CSM}}^{\text{b}}$	R_{out} (10^{15} cm)	$t_{\text{erupt}}^{\text{c}}$ (yr)	\dot{M} ($M_{\odot}\text{yr}^{-1}$)
iPTF15esb								
1	0.47	9.53	178.7	10.0	78.8	0.97	-	0.19–1.9
2	1.35	16.8	39.7	9.0	10.1	2.25	6.69	- ^d
3	1.77	39.6	120.0	6.2	4.1	5.5	16.34	- ^d
iPTF13dcc								
1	7.04	12.7	29.6	38.9	225.5	1.42	1.55	- ^d
2	17.23	25.5	44.67	27.6	12.14	6.94	21.72	- ^d

a. $M_{\text{CSM,th}}$ is the mass of optically thick CSM.

b. τ_{CSM} is the optical depth of CSM.

c. t_{erupt} is the time of the progenitor star erupting the CSM shells before explosion. Here we assume the velocity of the progenitor wind $v_w = 100 - 1,000$ km s⁻¹ and the shell expansion velocities $v_{\text{shell}} = 100$ km s⁻¹.

d. The shells were promptly expelled by some instability process and their mass-loss rates cannot be calculated.

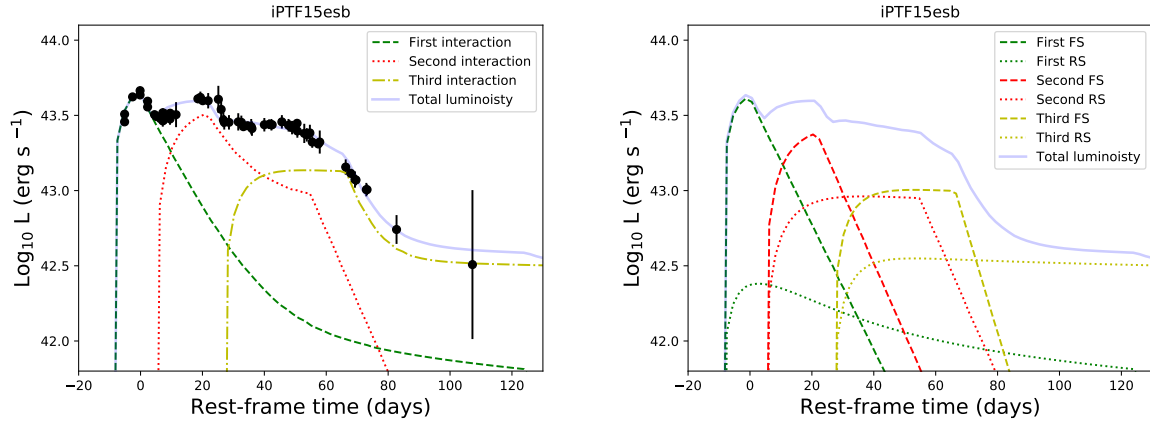


Fig. 1.— Left panel: The fit to the bolometric LC of iPTF15esb using the multiple ejecta-CSM interaction model. Data are obtained from Yan et al. (2017). Right panel: Separate contributions of the forward shocks and reverse shocks to the theoretical bolometric LC of iPTF15esb for successive interactions. The fitting parameters are shown in the text and Table 1.

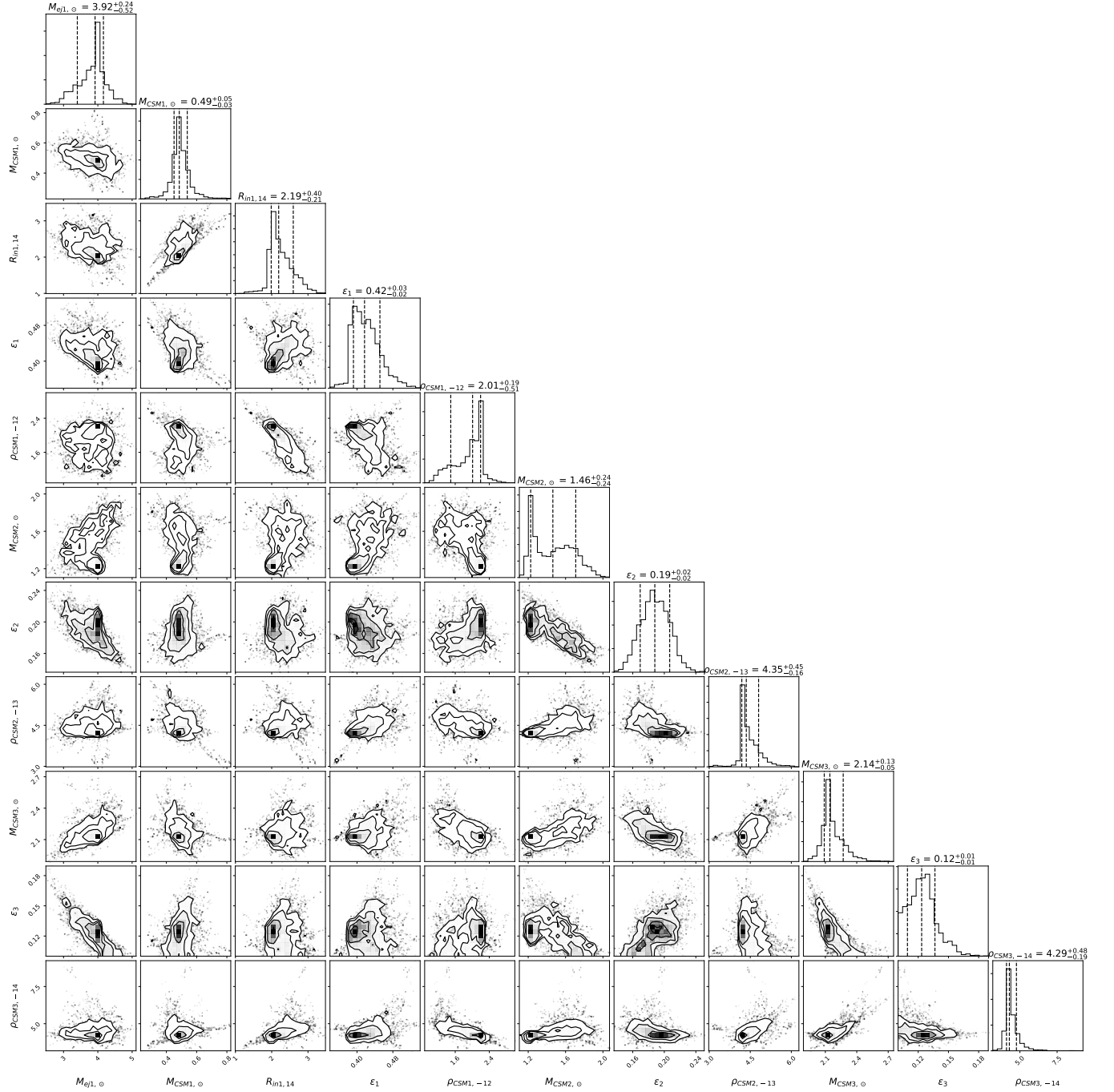


Fig. 2.— Corner plot of the parameters for fitting the LC of iPTF15esb. Medians and 1σ ranges are labeled.

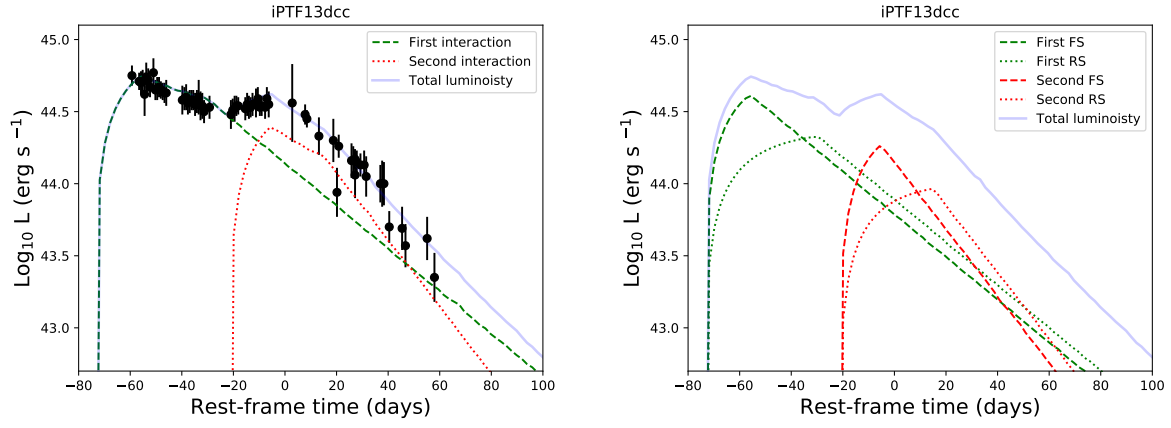


Fig. 3.— Same as in Figure 1 but for iPTF13dcc. Data are obtained from [Vreeswijk et al. \(2017\)](#). The fitting parameters are shown in the text and Table 1.

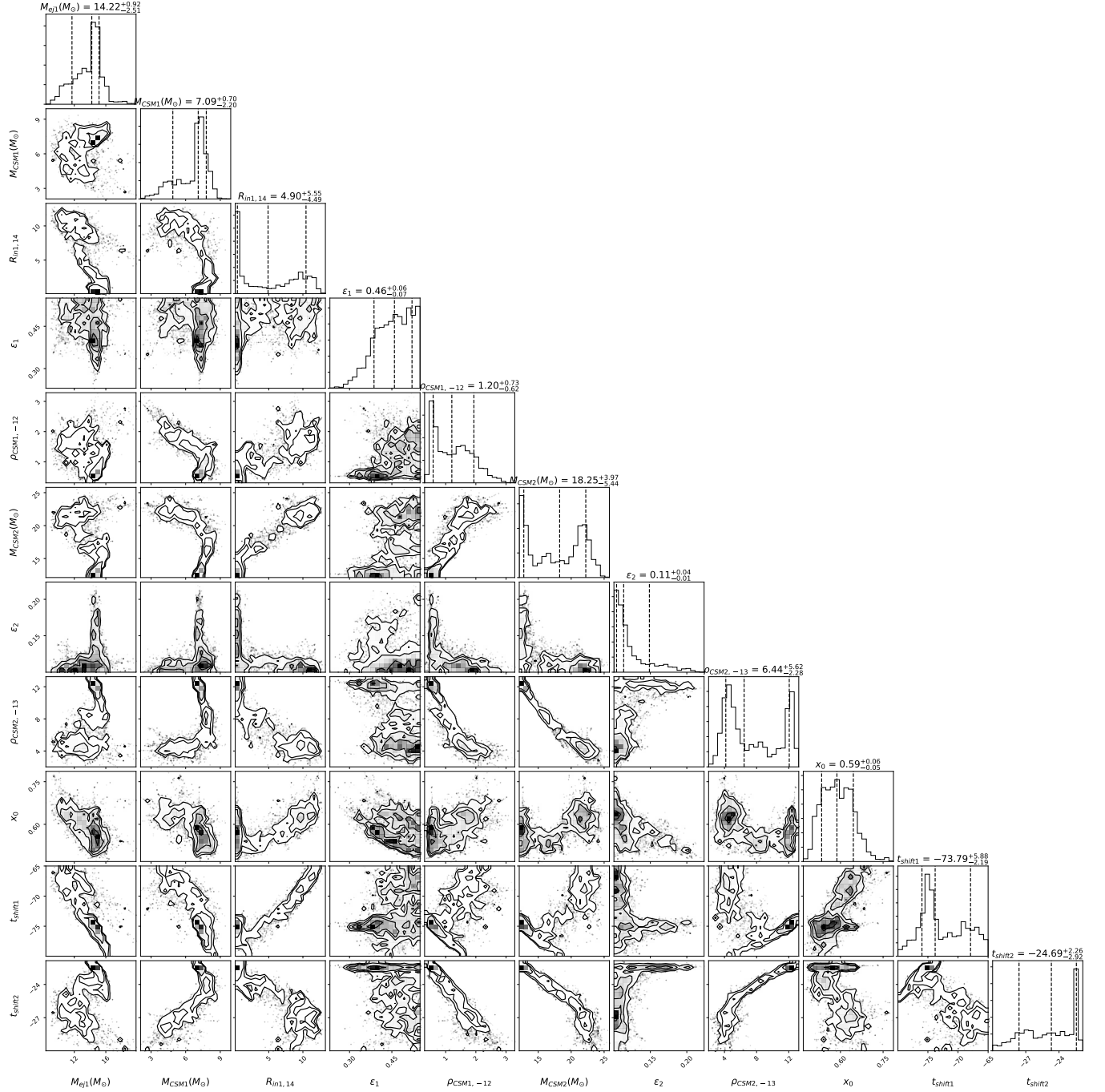


Fig. 4.— Corner plot of the parameters for fitting the LC of iPTF13dcc. Medians and 1 σ ranges are labeled.